Origin of Electrochemical, Structural and Transport Properties in Non-aqueous Zinc Electrolytes

Sang-Don Han,[ab] Nav Nidhi Rajput,[ac] Xiaohui Qu,[ac] Baofei Pan,[ab] Meinan He,[bd] Magali S. Ferrandon,[ab] Chen Liao,[ab] Kristin A. Persson[*ac] and Anthony K. Burrell[*ab]

[a]*Joint Center for Energy Storage Research, Argonne National Laboratory, Lemont, IL 60439, USA*
[b]*Chemical Sciences and Engineering Division, Argonne National Laboratory, Lemont, IL 60439, USA*
[c]*Environmental Energy Technologies Division, Lawrence Berkeley National Laboratory, Berkeley, CA 94720, USA*
[d]*Department of Mechanical Engineering, Worcester Polytechnic Institute, Worcester, MA 01609, USA*

Through coupled experimental analysis and computational techniques, we uncover the origin of anodic stability for a range of non-aqueous zinc electrolytes. By examining electrochemical, structural and transport properties of non-aqueous zinc electrolytes with varying concentrations, it is demonstrated that the acetonitrile-Zn(TFSI)$_2$, acetonitrile-Zn(CF$_3$SO$_3$)$_2$ and propylene carbonate-Zn(TFSI)$_2$ electrolytes can not only support highly reversible Zn deposition behavior on a Zn metal anode (≥99% of Coulombic efficiency), but also provide high anodic stability (up to ~3.8 V). The predicted anodic stability from DFT calculations is well in accordance with experimental results, and elucidates that the solvents play an important role in anodic stability of most electrolytes. Molecular dynamics (MD) simulations were used to understand the solvation structure (e.g., ion solvation and ionic association) and its effect on dynamics and transport properties (e.g., diffusion coefficient and ionic conductivity) of the electrolytes. The combination of these techniques provides unprecedented insight into the origin of the electrochemical, structural and transport properties in non-aqueous zinc electrolytes.

1. Introduction

Electrochemical, structural and transport properties of an electrolyte play a crucial role in defining the performance characteristics of energy storage technologies (e.g., batteries, fuel cells and supercapacitors), sensors, metal plating and many other applications.[1-7] Thus, it is of paramount importance to obtain fundamental understanding of electrolyte properties and behavior which govern (in part) application performance. The electrolytes, however, remain a poorly understood topic relative to the research devoted to other components and have undergone only minor changes for a long time holding back the progression of those applications. For example, the Li-ion battery, one of the most promising energy

storage technologies, have been developed for the last 30 years mostly focusing on the electrodes and recently the electrode/electrolyte interface, but it still faces several issues—limited performance, cost, aging and safety concerns which are mostly induced from limitation of the current state-of-the-art electrolyte—to apply in transportation and the electricity grid. With constant inflation in energy generation the future energy storage quest is rapidly moving towards high performance, safe and low cost batteries such as metal-air, multivalent and lithium-sulfur batteries, but the development of a comprehensive understanding of electrolyte interactions/properties and the exploration of new electrolyte solvents/salts are required to advance beyond-Li ion battery technologies.

As one of the potential candidates for a post-lithium-ion battery, non-aqueous multivalent (e.g., Mg^{2+}, Ca^{2+} and Zn^{2+}) metal cells provide an attractive opportunity in energy storage research due to higher theoretical volumetric capacity of a multivalent metal anode and the limited dendrite formation at the Mg metal anode.[8] The development of compatible multivalent electrolytes with a metal anode and reversible multivalent intercalation cathodes, however, is a significant challenge requiring an increased focus on fundamental understanding of electrolyte properties and behavior. For instance, in Mg metal cells various halides, halide-derivatives, BH_4 and BH_4-derivatives electrolytes are known to be compatible with Mg metal anode, but correlation between speciation and functionality is still under debate.[9-21] The compatibility of glyme-$Mg(TFSI)_2$ electrolyte with Mg metal is also controversial and generally a high overpotential and low Coulombic efficiency are observed in cell cycling.[21,22] In the case of Ca metal cells no electrolyte has been reported as compatible with reversible chemistry at a Ca metal anode.[23] We note that Ca has a very low standard free energy of oxide formation, lower even than Mg metal, compared to other metals as noted in a Ellingham diagram.[24] However, it appears that Zn^{2+} ion chemistry in Zn metal cells provides an exception among multivalent metals. Zn metal anodes coupled with a reversible intercalation cathode chemistry have a number of promising features: 1) highly efficient (≥99%) reversible Zn deposition on Zn metal anode in high performance non-aqueous Zn electrolytes (e.g., high anodic stability (maximum ~3.8 V) and ionic conductivity); 2) relatively lower activation barrier energy for migration of Zn^{2+} ions in a variety of cathode materials (e.g., $FePO_4$, NiO_2 and V_2O_5);[25] 3) similar ionic radius compared with Li^+ and Mg^{2+} ions[26] and 4) much higher volumetric capacity compared to other multivalent metals, such as Mg and Ca.[8] However, due to the high electrochemical potential of Zn metal, Zn cells are not considered a competitor compared to Li-ion energy storage. Nevertheless, the non-aqueous Zn system provides an opportunity to delve into the mechanisms in multivalent cell chemistry (e.g., reversible deposition on a metal anode and (de)intercalation into(from) a cathode material) and furthermore possibly solve the present issues in multivalent cell design and prototyping. From previous studies, it is apparent that the advent of multivalent batteries relies on the electrochemical, transport and structural properties of electrolytes. An enhanced understanding of non-aqueous Zn

electrolyte—electrochemical and transport properties (e.g., anodic stability, diffusion coefficient and ionic conductivity) and mechanisms at an electrolyte/electrode interface—can aid in understanding the correlation between the atomistic structure of the electrolyte and its performance by utilizing experimental analysis combined with classical molecular dynamics and DFT calculations. As shown in previous studies,[27-33] the molecular-level solvation structure (ion solvation and ionic association behavior) and dynamics of the bulk electrolytes are not only crucial factors influencing the bulk electrolyte properties and elucidate mechanisms at an electrolyte/electrode interface, but also critical design metrics for novel electrolytes.

Most of the previous rechargeable Zn cell studies have been performed using aqueous Zn electrolytes, such as $Zn(NO_3)_2$ and/or $ZnSO_4$, with various types of MnO_2 or copper hexacyanoferrate (CuHCF) nano-cube cathodes, which mostly focus on the structural and electrochemical properties of cathode materials, reversible intercalation mechanism and cycle life performance for the Zn metal cells.[34-40] On the other hand, in 1987 R. Schöllhorn *et al.* reported the intercalation of Zn^{2+} ion by electron/ion transfer reactions into the Chevrel-type molybdenum cluster chalcogenides Mo_6X_8 (X = S, Se) in non-aqueous electrolytes (i.e., $Zn(ClO_4)_2$ in acetonitrile (AN) or propylene carbonate (PC)) demonstrating the competitive influence of electronic and steric factors upon these processes.[41] As new rechargeable Zn electrolytes, the binary room temperature molten electrolyte based on acetamide and $Zn(ClO_4)_2$[42] and the dicyanamide ionic liquids-based electrolytes[43] were characterized and evaluated with the γ-MnO_2/Zn and Zn/Zn cells, respectively. K. Zaghib *et al.* recently demonstrated cycling performance of a Zn/PANi (polyaniline) cell with a non-aqueous PC-$Zn(TFSI)_2$ electrolyte.[44] Remarkably, most previous studies on Zn^{2+} ion (de)intercalation mechanism or rechargeable Zn battery have been performed in aqueous Zn electrolyte system, while very little information is available in the literature on non-aqueous Zn battery, in particular non-aqueous Zn electrolytes.

Hence, this study aims to scrutinize in detail the general electrochemical and transport properties (e.g., reversible Zn metal deposition behavior with Coulombic efficiency, overpotential, anodic stability, diffusion coefficient and ionic conductivity) of non-aqueous Zn electrolytes—consisting of mixtures of Zn salts (e.g., $Zn(PF_6)_2$, $Zn(TFSI)_2$, $Zn(BF_4)_2$ and $Zn(CF_3SO_3)_2$) and organic solvents (e.g., diglyme, propylene carbonate, acetonitrile and *N*,*N*-dimethylformamide). Classical molecular dynamics simulations are utilized to complement the experimental work and to provide insights into the molecular-level ion solvation/ionic association behavior, dynamics of the bulk electrolytes and the relationship between solution structure and transport properties of bulk electrolytes. In addition, electrochemical stability windows of the different included species—both salt anions as well as solvents—are predicted via adiabatic ionization potential(IP) DFT calculations.

2. Experimental and computational methods

2.1. Materials and electrolyte preparation

The zinc salts and solvents used in the present study and their acronyms/schematics are noted in Fig. 1. Zinc carbonate basic ($[ZnCO_3]_2 \cdot [Zn(OH)_3]$), tetrafluoroboric acid (HBF_4, 48 wt. % in H_2O), zinc chloride ($ZnCl_2$), and silver hexafluorophosphate ($AgPF_6$) were purchased from Sigma-Aldrich and Alfar Aesar. The synthesis of $Zn(BF_4)_2$ and $Zn(PF_6)_2$ are following literature procedures.[45,46] The 2.75 g of zinc carbonate basic ($[ZnCO_3]_2 \cdot [Zn(OH)_2]_3$, 25 mmol of Zn) was suspended in 250 mL deionized water in a 500 mL round bottom bottle, to which was added 8.2 g of tetrafluoroboric acid solution (HBF_4, 48 wt. % in H_2O, 45 mmol of HBF_4) slowly over 30 minutes. After the bubbling stopped, the mixture was further stirred at room temperature overnight to confirm complete reaction. The mixture was then filtered through a Celite® (Sigma-Aldrich) overnight. Removal of water solvent from the collected colorless solution via a Rotavapor evaporator afforded pure $Zn(BF_4)_2$ as white solid (4.0 g, 74.4% yield). The purity of salt was confirmed by ^{19}F NMR in CH_3CN, recorded at -149.5 ppm, referenced to $Et_2O \cdot BF_3$ at -153 ppm. The salt was then dried under vacuum at room temperature overnight, which followed additional drying of $Zn(BF_4)_2$ at 80˚C under vacuum in an argon-filled glove box for more than 24 hours before use. In an argon-filled glove box, 490 mg of zinc chloride ($ZnCl_2$, ≥98%, Sigma-Aldrich) (3.6 mmol of Zn) was suspended in 20 mL of anhydrous acetonitrile (CH_3CN, 99.8%, Sigma-Aldrich), to which was added a mixture, 1.77 g of silver hexafluorophosphate ($AgPF_6$, 98%, Sigma-Aldrich) (7.0 mmol of Ag) in 20 mL of anhydrous acetonitrile, slowly over 10 minutes. The mixture was allowed to stir at room temperature in dark for 12 hours to ensure the completion of the reaction. After stirring, the clear solution was collected via filtration through a Celite®. Removal of acetonitrile from the solution under Schlenk line afforded white solid of analytically pure $Zn(PF_6)_2$ (430 mg, 34.6% yield). The salt was then dried under vacuum at room temperature in an argon-filled glove box for more than 24 hours before use.

$Zn(TFSI)_2$ (Solvionic, 99.5%) and $Zn(CF_3SO_3)_2$ (Sigma-Aldrich, 98%) were used after drying at 90˚C in a vacuum oven. Anhydrous G2 (Sigma-Aldrich, 99.5%), PC (Sigma-Aldrich, 99.7%), AN (Sigma-Aldrich, 99.8%) and DMF (Sigma-Aldrich, 99.8%) were used after overnight drying with completely dried molecular sieves (Sigma-Aldrich, 4 Å, 8-12 mesh). Appropriate ratios of zinc salts and solvents were mixed together in hermetically sealed glass vials and stirred on a hot plate to form homogeneous solutions. All materials were handled in an argon-filled inert atmosphere glove box (<0.5 ppm H_2O and <0.5 ppm O_2). The water content of the mixtures was verified to be <30 ppm using a Mettler Toledo DL39 Karl Fischer coulometer.

2.2. Electrochemical measurements and morphology characterization

Cyclic voltammetry (CV) and linear sweep voltammetry (LSV) measurements of the prepared electrolytes were performed in a three-electrode cell inside the glove box using a Parstat MC potentiostat (Princeton Applied Research). The zinc wires (Alfa Aesar, 99.95 %, 2.0 mm diameter) polished with a sand paper were used as the reference and the counter electrodes, and a Pt disk (CH Instruments, 2.0 mm diameter) was used as the working electrode. Conductivity values were measured in 20˚C steps from -20˚C to 60˚C using an Orion 3 Star conductivity meter (Thermo Scientific) with a MI-915 dip-type conductivity probe (Microelectrodes, Inc.), which is one of the integrated tools on Freeslate's robotic platform (CM3, Freeslate Inc.) in a custom-built nitrogen-filled glove box (MB 200B, MBraun). In each measurement, the probe was washed with anhydrous methanol (Sigma Aldrich, 99.8%) and dried over adsorbing mats to avoid cross contamination. The probe was regularly calibrated with standard solutions (0.1, 1, 5, 10, and 20 mS cm^{-1}, Ricca Chemical) at 25˚C. The error on the reported conductivities is estimated to be ± 5%. The diffusion coefficient was estimated by the chronoamperometry technique using the same three-electrode cell used in CV or LSV measurements. The electrode potential was held at - 0.5 V *vs.* Zn/Zn^{2+} for 70 s. Current as a function of time was recorded using a Parstat MC potentiostat, and Coulombic charge was calculated by integrating current with respect to time. The diffusion coefficient was calculated according to the following equation:

$$Q = \frac{2nFAC_0D^{1/2}}{\pi^{1/2}} t^{1/2} + Q_{dl} + Q_{ads} \quad (1)$$

where Q is the total Coulombic charge (C) for Zn deposition, n is the number of electrons transferred, F is the Faraday constant (C mol^{-1}), A is the electrode area (cm^2), C_0 is the bulk Zn ion concentration (mol/cm^3), D is the Zn ion diffusion coefficient in the electrolyte (cm^2 s^{-1}), t is time (s), Q_{dl} is the double-layer charge, and Q_{ads} is the charge associated with the adsorbed species.[47]

Hitachi S4700 scanning electron microscope with an energy dispersive X-ray spectrometer (SEM-EDS) was used to characterize the morphology and to investigate the elements of deposited materials on a Pt electrode. To obtain deposited materials, chronopotentiometric technique was utilized for a Pt electrode in different non-aqueous Zn electrolytes at - 0.5 mA constant current overnight.

2.3. MD simulations and DFT calculation

Classical molecular dynamics (MD) simulations were performed using the GROMACS MD simulation package version 4.5.3.[48] Initial cubic simulation boxes with periodicity in the XYZ directions were constructed for the $Zn(TFSI)_2$ and $Zn(CF_3SO_3)_2$ salts in G2, AN, PC and DMF solvents at 0.1 M and 0.5 M concentrations using PACKMOL.[49] All initial configurations were subjected to two steps energy minimization, first using steepest descent with the convergence criteria of 1000 kcal/mol Å followed by

conjugated-gradient energy minimization with convergence criteria of 10 kcal/mol Å. After minimization isothermal-isobaric (NPT) simulations were performed at 298 K and 1 bar using the Berendsen barostat with a time constant of 0.1 ps to get the correct density. All systems are then heated to a temperature of 400 K for 1 ns followed by a 3ns annealing to 298 K in a canonical ensemble (NVT) using an improved velocity rescaling algorithm with a coupling constant of 0.1 ps to ensure that the molecules were not trapped in a metastable state. Afterwards, NVT simulations were performed for 10ns to equilibrate the systems at 298 K. The simulations are long enough to capture the structural and dynamical properties of equilibrated systems. Structural and dynamical properties were averaged over two independent configurations of the same system. The bonded and non-bonded parameters were obtained using generalized amber force fields (GAFF) and the partial charges were obtained with the RESP procedure using Antechamber.[50-52] Long range electrostatic interactions were handled by the Particle-mesh Ewald (PME) method with a cut-off of 1.2 nm and the Lennard-jones interaction was truncated at 1.2 nm. The diffusion coefficient was computed by a least square fitting a straight line through a mean square displacement in the diffusive regime. The conductivity is computed using the Nernst-Einstein(NE) equation as follows, where N_{pair} is the number of ion pairs, q_+ and q_- are the total charges on cation and anion respectively, D_+ and D_- are the self diffusion coefficients of cation and anion respectively, V is the simulation box volume, T is the temperature, k_β is the Boltzmann constant:

$$\sigma_{NE} = \frac{N_{pair}}{VTk_\beta}(q_+^2 D_+ + q_-^2 D_-) \quad (2)$$

DFT calculations were performed using the QChem 4.1 package.[53,54] All the species are fully relaxed at the B3LYP/6-31+G* level.[55,56] Vibrational frequency calculations were carried out for each stationary point to check the character of the stationary point, as a true minimum should have no imaginary frequencies. All final geometries are confirmed as true minima by iteratively adjusting the structures. The single point energy is evaluated at the same theoretical level. The solvent effect is taken into account by the IEF-PCM dielectric continuum model.[57] All the calculations were carried out automatically by a workflow infrastructure developed by the Electrolyte Genome project.[58] Ionization potentials (IP)[59]—the energy to oxidize a compound as calculated by the energy difference between the oxidized and the original state—were calculated to predict the anodic stability of the electrolyte components. To identify the limiting components of the electrolyte electrochemical stability, we calculated the stability of both anions and solvents. Guided by the molecular dynamics calculations, the anion IP calculation utilized the solvation structure of an Zn-anion ion pair for all systems, except that of DMF-$Zn(TFSI)_2$ since ion pairing (see section 3.3) was found to be the prevailing solvation structure for the considered systems and concentrations.

3. Results and Discussion

3.1. Zn metal plating/stripping behavior and deposition morphology

The Figs. 2a-2c represents the CVs of the AN-Zn(TFSI)$_2$, AN-Zn(CF_3SO_3)$_2$ and PC-Zn(TFSI)$_2$ electrolytes with varying concentration to evaluate the Zn plating/stripping behavior, Coulombic efficiency, overpotential and the electrochemical window. In Figs. 2a-2c, the cathodic currents below 0 V and the anodic peak around the open-circuit voltage (OCV) are related to Zn deposition and dissolution, respectively. The AN-Zn(TFSI)$_2$, AN-Zn(CF_3SO_3)$_2$ and PC-Zn(TFSI)$_2$ electrolytes show reversible Zn deposition behavior with negligible or no additional redox reaction and wide electrochemical window up to approximately 3.7 V, 3.5 V and 3.4 V, respectively (Fig. 2d, for 0.5 M concentration), suggesting that those mixtures can be used as potential electrolytes with a variety of cathode materials in rechargeable Zn batteries. It is noteworthy that all three electrolytes have the highest current values for 0.5 M concentration (possibly due to solubility limit), which can be selected as the standard concentration for further study. Additional CVs and LSVs for the 0.1 M electrolytes composed of one of the zinc salts (i.e., Zn(TFSI)$_2$, Zn(BF_4)$_2$, Zn(PF_6)$_2$ and Zn(CF_3SO_3)$_2$) and one of the organic solvents (i.e., G2, PC, AN and DMF) are demonstrated in Supporting Information (Figs. S1-S4). In Figs. S1-S4, the current for several electrolytes exhibits minimal change on cycling (e.g., G2-Zn(TFSI)$_2$, G2-Zn(CF_3SO_3)$_2$, DMF-Zn(BF_4)$_2$ and DMF-Zn(PF_6)$_2$), possibly due to the reaction of the uncoordinated solvent present in the electrolyte with the freshly plated Zn metal.[60] Most other electrolytes, such as G2/DMF-Zn(TFSI)$_2$, G2/PC/DMF-Zn(CF_3SO_3)$_2$, AN/PC/DMF-Zn(BF_4)$_2$ and G2/AN/PC/DMF-Zn(PF_6)$_2$, also show the electrochemical plating/stripping behavior of Zn, but there are additional large and/or small peaks which indicate additional reversible and/or irreversible redox reactions. In addition, those electrolytes have relatively narrower electrochemical windows (Figs. S1-S4). The CV of the G2-Zn(BF_4)$_2$ electrolyte is characterized by featureless cathodic and anodic currents, probably due to highly-limited solubility of Zn(BF_4)$_2$ salt in G2, which can also be deduced from relatively low current values (Fig. S3a).

The Coulombic efficiency of Zn deposition/dissolution behavior from CVs is summarized in Table 1. Coulombic efficiency for most electrolytes is not available because the Zn plating/stripping peaks overlap with additional redox reaction peaks. Only 0.1 M DMF-Zn(TFSI)$_2$ electrolyte shows approximately 50.8 Coulombic efficiency, while other electrolytes, including the AN-Zn(TFSI)$_2$, PC-Zn(TFSI)$_2$ and AN-Zn(CF_3SO_3)$_2$ electrolytes, show ≥99 % Coulombic efficiency for varying concentrations (Fig. 2a-2c) which suggests very high reversibility of Zn deposition/dissolution. The Figs. 2e and 2f demonstrate the reversible deposition overpotential for the variable-concentration AN-Zn(TFSI)$_2$ electrolytes and the 0.5 M AN-Zn(TFSI)$_2$, AN-Zn(CF_3SO_3)$_2$ and PC-Zn(TFSI)$_2$ electrolytes, respectively. Additional results of reversible deposition overpotential for the variable-concentration AN-Zn(CF_3SO_3)$_2$ and PC-Zn(TFSI)$_2$ electrolytes are represented in Fig. S5. After 5 cycles, the overpotential values are almost consistent for

additional 15 cycles and are decreased with increase of concentration (Figs. 2e and S5). In Fig. 2f, the reversible deposition overpotential of 0.5 M AN-$Zn(TFSI)_2$ is the highest (~0.1 V), 0.5 M AN-$Zn(CF_3SO_3)_2$ the next (~0.07 V) and 0.5 M PC-$Zn(TFSI)_2$ the lowest (~0.06 V).

Typical SEM micrographs and the corresponding EDS spectrum of the deposited materials on the Pt electrodes are shown in Fig. 3. The Figs. 3a, 3c and 3e provide overviews of the Zn deposited Pt electrodes in three selected non-aqueous Zn electrolytes (i.e., AN-$Zn(TFSI)_2$, AN-$Zn(CF_3SO_3)_2$ and PC-$Zn(TFSI)_2$) under a lower magnification, while Figs. 3b, 3d and 3f show the morphologies of selected zones (i.e., α, β and γ) of each overview. The morphologies represent deposited Zn nanolines with approximately 100 nm diameter, which were possibly obtained from a nuclear-growth kinetic process of the Zn on the Pt electrodes. The inset images in Figs. 3b, 3d and 3f show the EDS spectrum for the deposited materials, in which Lβ_1, Kα_1 and Kβ_1 characteristic peaks on around 103.5, 863.7 and 957.0 ev, respectively, correspond to the Zn element. Both surface topography and EDS spectrum analysis indicate that only Zn is readily deposited on the Pt electrodes in all three selected electrolytes by utilizing chronopotentiometric technique, which is in accord with apparent Zn metal plating behavior observed from previous CVs (Fig. 2). Based upon the analysis of CVs and LSVs of the electrolytes (Figs. 2 and S1-S4) and morphologies and EDS spectrum of the deposited materials (Fig. 3), it appears that select non-aqueous Zn electrolytes show highly-efficient ($\geq$ 99%) reversible deposition behavior on a Zn metal anode with wide electrochemical window (up to ~3.8 V), which can provide possible utilization of those electrolytes in non-aqueous Zn metal cells.

3.2. Electrochemical stability and elucidation of its limiting factors

The oxidation of a non-aqueous electrolyte is a crucial issue when high potential cathodes are used for the development of high energy density batteries based on polar aprotic electrolyte solutions.[61] Most of the non-aqueous solvents and salts of interest are possibly oxidized at high potentials, and thus their intrinsic anodic behavior is important for further studies. The anodic stability of each 0.1 M electrolyte was obtained from LSVs measurements (Figs. S1-S4) and summarized in Table 1. As shown in the CV plots (Figs. S1b, S1c and S2b), the LSVs confirm higher anodic stability of the 0.1 M AN-$Zn(TFSI)_2$, AN-$Zn(CF_3SO_3)_2$ and PC-$Zn(TFSI)_2$ electrolytes as 3.8 V, 3.6 V and 3.4 V, respectively compared to those of other electrolytes (Figs. S1-S4). It is noteworthy that anodic stability of an electrolyte reduces with increasing concentration (insets of Figs. 2a-2c): approximately 0.15 V for the AN-$ZN(TFSI)_2$, 0.1 V for the AN-$Zn(CF_3SO_3)_2$ and 0.17 V for the PC-$Zn(TFSI)_2$ electrolytes. In addition, it is interesting to note that a trend can be observed based on different solvents: the range of high voltage limit with varying Zn salts is approximately 3.6 - 3.8 V *vs*. Zn/Zn^{2+} for AN, 3.3 - 3.4 V *vs*. Zn/Zn^{2+} for PC, 2.5 - 2.9 V *vs*.

Zn/Zn^{2+} for DMF and 2.3 - 2.6 V *vs*. Zn/Zn^{2+} for G2 (Table 1). This indicates the following order for decreasing anodic stability in 0.1 M non-aqueous zinc electrolytes:

$$AN\text{-}Zn(X)_2 > PC\text{-}Zn(X)_2 > DMF\text{-}Zn(X)_2 \geq G2\text{-}Zn(X)_2 \ (X = TFSI^-, CF_3SO_3^-, BF_4^- \text{ and } PF_6^-)$$

which suggests that a solvent is one of the most important factors in determining the electrochemical window of non-aqueous Zn electrolytes.

The DFT predicted anodic stability (IP) is shown in Fig. 4. In each electrolyte, the anodic stability limit is determined by either the solvent or the anion—whichever is lower. For the 0.1 M AN-$Zn(TFSI)_2$, AN-$Zn(CF_3SO_3)_2$ and PC-$Zn(TFSI)_2$ electrolytes, the lowest anodic limit is above 4.0 V which is roughly consistent with experimental results that no oxidation reaction is observed until approximately 3.8 V, 3.6 V and 3.4 V, respectively. Except for the AN-$Zn(TFSI)_2$ and PC-$Zn(TFSI)_2$ electrolytes, the anions are predicted to have a higher anodic limit than the solvents. It means that the anodic stability of AN-$Zn(TFSI)_2$ and PC-$Zn(TFSI)_2$ electrolytes is mostly limited by the $TFSI^-$ anion, while the solvent is the predominant limiting factor for the anodic stability of the other electrolytes. The anodic stability of the electrolytes decreases in the order of AN ≥ PC > DMF ≥ G2, which is in good agreement with the experimental trend. Previous studies on anodic stability for a variety of non-aqueous systems highlights the salt, the electrode materials and impurities as potential stability-limiting factors governing the onset of the oxidation reactions, however the anodic reactions of polar aprotic systems and their mechanism are unclear.[61] From our study, of non-aqueous zinc electrolyte systems, it appears that the solvent is a dominant factor in determining the anodic stability, and only AN-$Zn(TFSI)_2$ and PC-$Zn(TFSI)_2$ are governed by the stability of the salt anion.

3.3. Ion solvation and ionic association

The solvation structure (e.g., ion solvation and ionic association) is one of the important factors, as it provides a link between the molecular-level interactions and electrolyte properties such as diffusion coefficient and ionic conductivity. The Zn-anion, Zn-solvent and anion-solvent radial distribution function g(r), thus, was computed to understand the local solvation structure of the electrolyte. The g(r) and snapshots of all computed systems are provided in Supporting Information (Figs. S6-S13). The first solvation shell around Zn^{2+} consists of oxygen from $TFSI^-$ or $CF_3SO_3^-$ anion and/or solvent molecules at ~ 2.2 Å. The Zn-solvent g(r) shows peak from Zn-O(DMF) and Zn-O(PC) at 2.2 Å and Zn-O(G2) at 2.1 Å, whereas Zn-N(AN) peak is observed at 2.3 Å (Fig. S14). Among the four solvents considered in this work, small size O-donor solvents (i.e., DMF, PC and G2) show the stronger interaction with Zn^{2+} as compared to N-donor solvents (i.e., AN), which indicates the following order of DMF > PC ~ G2 > AN for the strength of Zn-solvent interaction in the $Zn(TFSI)_2$ electrolytes and DMF ~ PC > G2 > AN in the $Zn(CF_3SO_3)_2$ electrolytes (Fig. S14). Fig. 5 shows the coordination numbers (CN) of the Zn-anion and

Zn-solvent for 0.1 M and 0.5 M of $Zn(TFSI)_2$ and $Zn(CF_3SO_3)_2$ electrolytes with DMF, PC, G2 and AN. The CN was computed by integrating g(r) in the first solvation shell, which consists of oxygen or nitrogen from $TFSI^-$ or $CF_3SO_3^-$ anion and/or solvent molecules. For the Zn-anion coordination, the CN is computed by integrating g(r) between Zn^{2+} and N($TFSI^-$) and Zn^{2+} and S($CF_3SO_3^-$), while the CN in Zn-solvent coordination is computed from g(r) between Zn^{2+} and N(AN), Zn^{2+} and O(DMF), Zn^{2+} and O(PC) and Zn^{2+} and O(G2). The small size linear O-donor solvents exhibit better dissociating capability (between cations and anions) than the cyclic solvent of PC and N-donor solvent of AN. As previously reported for Mg electrolytes,[36] the dissociation of cation-anion is not directly proportional to dielectric constant of solvents: even though G2 has a much smaller dielectric constant, its high O-donor denticity and ability to wrap around cation promote dissociation between the cation and anion. Relatively weaker interaction between Zn^{2+} cations and AN solvent molecules results in formation of aggregates (AGGs) in the solution.

In Fig. 5, the CNs of Zn-TFSI and Zn-CF_3SO_3 are similar for the 0.1 M and 0.5 M of AN- and PC-based electrolytes, while the CNs of Zn-TFSI are smaller than those of Zn-CF_3SO_3 in DMF- and G2-based electrolytes. The molecular-level interaction between those solvent molecules and the anions were investigated to verify this difference. Fig. S15 shows that in all solvents the $CF_3SO_3^-$ anions have relatively stronger interaction with solvent molecules as compared to $TFSI^-$ anions possibly due to the steric hindrance and more dispersed charge of the $TFSI^-$ anions. Similar trends have been observed previously for lithium salts.[28,62] The increase in CNs of the Zn-anion and decrease in CNs of the Zn-solvent are observed with increasing concentration from 0.1 M to 0.5 M. The increase in CNs of the Zn-anion with increasing concentration may affect the stability of an electrolyte if the ion-paired anions become unstable in the solution,[33] which can be observed in experimental results (Figs. 2a-2c). The decrease in CNs of the Zn-solvent is the least for G2, which showcases its strong chelating effect around Zn^{2+} with O-donor denticity. Based upon the detailed understanding of electrolyte mixtures including how interactions at the molecular-level are affected by factors such as solvent/ion structure and concentration, the relationship between the molecular-level interactions and electrolyte properties will be addressed in the following section.

3.4. Dynamical, transport, electrochemical properties

The isothermal diffusion coefficients (at 25˚C) of the 0.1 M electrolytes composed of $Zn(TFSI)_2$ or $Zn(CF_3SO_3)_2$ salts with four different solvents (e.g., AN, DMF, PC and G2) were estimated using equation (1) with the integrated values from chronoamperometry technique (Fig. 6a) and were simulated from mean square displacement of ions (Figs. 6b and 6c). The trends observed in diffusion coefficient values from simulations are in good agreement with experimental results, while the quantitative

agreement is difficult due to limitation of non-polarizable force field used in this work. Among the four different solvent-based electrolytes, the AN-based electrolytes have the highest diffusion coefficient values and the DMF-based electrolytes show the second highest diffusion coefficient values compared to those of the PC- and G2-based electrolytes (Fig. 6a). The MD simulations also indicate the same trend for the different solvents (Fig. 6b and 6c). It appears that a solvent with high dielectric constant, weaker coordination with Zn^{2+} and more dispersed charge may result in faster dynamics of both cation and anion. G2 shows better solvation of Zn-anion compared to PC, but its low dielectric constant and stronger chelating effect result in slower dynamics of the ions. On the other hand, a high dielectric constant, weakly coordinating and small sized molecule, such as AN, provide better mobility to both cation and anions. Even though the dielectric constant of PC (ε = 60) is higher than AN (ε = 37.5) and DMF (ε = 36.7), the mobility of cations and anions is the fastest in AN followed by DMF and the slowest in PC for both $Zn(TFSI)_2$ and $Zn(CF_3SO_3)_2$ salts possibly due to viscosity difference in each solvent (AN = 0.37 mPa·s, DMF = 0.79 mPa·s and PC = 2.50 mPa·s at 25˚C).[63,64] This trend is in agreement with previously reported experimental results for $LiClO_4$, where the fastest dynamics is observed in AN followed by DMF and the slowest dynamics in PC.[65] This suggests that dynamics of ions is not simply proportional to dielectric constant, but determined by more complicated factors, such as donor atoms of a solvent, molecular geometry and strength of interaction with cation and anion. DMF has stronger interaction with Zn^{2+} of $Zn(TFSI)_2$ than Zn^{2+} of $Zn(CF_3SO_3)_2$, which contribute to more strongly solvated Zn^{2+} with slower dynamics and more uncoordinated $TFSI^-$ with faster dynamics. In the case of AN-based electrolytes, the diffusion coefficient of Zn ion for $TFSI^-$ anion is relatively higher than that for $CF_3SO_3^-$ anion (Fig. 6), probably due to an association tendency of the anions (i.e., anion…Zn^{2+} cation coordination)—$TFSI^-$ anions, proposed to be a highly dissociated anion, have more coordination with the solvent molecules resulting in the higher diffusivity compared to possibly highly associated $CF_3SO_3^-$ anions—reported in previous electrolyte solvation and ionic association studies for the AN-Li(X) electrolytes (X = PF_6^-, FSI^-, $TFSI^-$, ClO_4^-, $DFOB^-$, BF_4^-, $CF_3CO_2^-$ and $CF_3SO_3^-$).[27-32]

The isothermal ionic conductivities (at 298 K) of 0.1 M $Zn(TFSI)_2$ and $Zn(CF_3SO_3)_2$ electrolytes with AN, DMF, PC and G2 were computed using equation (2) (Fig. 7a). The trend in ionic conductivities (AN > DMF > PC > G2) is in accordance with experimental results (Fig. S16) and inferences from previous diffusion coefficient values (Fig. 6). Faster dynamics and more charged pairs in AN solutions show relatively higher conductivities compared to DMF-, PC- and G2-based electrolytes. Fig. 7b demonstrates the experimentally measured isothermal ionic conductivity values (at 20˚C) for the AN-$Zn(TFSI)_2$ electrolytes, along with values for the corresponding mixtures with another Zn salt (i.e., AN-$Zn(CF_3SO_3)_2$) or solvent (i.e., PC-$Zn(TFSI)_2$) for comparison. It is interesting to note that the AN- and PC-$Zn(TFSI)_2$ electrolytes exhibit a peak in ionic conductivity near the concentration of 0.5 M, which is not the case for

other Li salt electrolytes with aprotic solvents,[29,66] while the ionic conductivity of the AN-$Zn(CF_3SO_3)_2$ electrolytes peaks near a concentration of 1.0 M (Fig. 7b). The explanation for this may lie in solubility limit, noted above from solubility observation in Table 1: both AN- and PC-$Zn(TFSI)_2$ electrolytes are lightly cloudy solutions even at 0.1 M, while AN-$Zn(CF_3SO_3)_2$ electrolyte is a homogeneous solution. For the concentration range (0.1 - 1.0 M) at room temperature (20˚C), the conductivity of the AN-$Zn(TFSI)_2$ electrolyte is remarkably higher than the values for the electrolytes with another salt, $Zn(CF_3SO_3)_2$, or solvent, PC (Fig. 7b), which may be expected considering the diffusion coefficient values for the AN-$Zn(TFSI)_2$ electrolyte in Fig. 6. The variation with temperature of the ionic conductivities of the 0.5 M $Zn(TFSI)_2$ and $Zn(CF_3SO_3)_2$ electrolytes with four different solvents are given in Fig. S16. Unlike other electrolytes, the ionic conductivities of the AN-$Zn(TFSI)_2$ and -$Zn(CF_3SO_3)_2$ electrolytes are almost the same or minor increase with increasing temperature (≥ 20˚C for the AN-$Zn(TFSI)_2$ and AN-$Zn(CF_3SO_3)_2$ electrolytes) possibly due to relatively lower boiling point of AN (82˚C). The behavior shown in Fig S16 for different solvents is in accord with the above noted diffusion coefficient values for the electrolytes (Fig. 6). The conductivity data were reproduced with samples prepared from different batches of Zn salts and the water content of the electrolytes was verified to be negligible.

4. Conclusions

The electrochemical, transport and dynamical properties of non-aqueous zinc electrolytes have been examined in detail by employing several modes of experimental evaluation in concert with MD simulations and DFT calculations. Among a variety of electrolytes, the AN-$Zn(TFSI)_2$, PC-$Zn(TFSI)_2$ and AN-$Zn(CF_3SO_3)_2$ electrolytes represent highly-efficient (≥ 99%) reversible deposition behavior on a Zn metal anode with wide electrochemical window (up to 3.6 V for 0.5 M concentration), which can provide possible utilization of those electrolytes in non-aqueous zinc metal cells. Based upon experimental analysis and DFT calculations for the anodic stability of electrolytes, we identify that the solvent as the most important factor in determining the anodic stability of most zinc electrolytes except for the case of $Zn(TFSI)_2$ where the $TFSI^-$ anion sets the upper voltage limit due to its relatively lower anodic stability. The solvation structure and dynamical/transport/electrochemical properties analysis demonstrate weakly coordinated solvents with high dielectric constants, such as AN, promote formation of large complexes with faster dynamics and low partial charge which can dissociate easily resulting in higher conductivity. In the case of AN-based electrolytes, the diffusion coefficient of Zn ion for $TFSI^-$ anion, proposed to be a highly dissociated anion, is relatively higher than that for $CF_3SO_3^-$ anion, possibly highly associated anion, which results in relatively higher conductivity of the AN-$Zn(TFSI)_2$ electrolyte.

Acknowledgments

This work was supported as part of the Joint Center for Energy Storage Research (JCESR), an Energy Innovation Hub funded by the U.S. Department of Energy, Office of Science, Basic Energy Sciences. The submitted manuscript has been created by UChicago Argonne, LLC, Operator of Argonne National Laboratory ("Argonne"). Argonne, a U.S. Department of Energy Office of Science laboratory, is operated under Contract No. DE-AC02-06CH11357. High performance computational resources for this research were provided by the National Energy Research Scientific Computing Center, which is supported by the Office of Science of the U.S. Department of Energy under Contract No. DE-AC02-05CH11231. The Materials Project (BES DOE Grant No. EDCBEE) is acknowledged for infrastructure and algorithmic support.

References

1 K. Xu, *Chem. Rev.*, 2004, **104**, 4303.

2 P. Simon and Y. Gogotsi, *Nat. Mater.*, 2008, **7**, 845.

3 J. W. Fergus, *Sens. Actuators, B*, 2008, **134**, 1034.

4 Y. Wang, K. S. Chen, J. Mishler, S. C. Cho and X. C. Adroher, *Appl. Energy*, 2011, **88**, 981.

5 S. Dimitrijević, M. Rajčić-Vujasinović and V. Trujić, *Int. J. Electrochem. Sci.*, 2013, **8**, 6620.

6 K. Xu, *Chem. Rev.*, 2014, **114**, 11503.

7 C. Zhong, Y. Deng, W. Hu, J. Qiao, L. Zhang and J. Zhang, *Chem. Soc. Rev.*, 2015, DOI: 10.1039/C5CS00303B.

8 J. Muldoon, C. B. Bucur and T. Gregory, *Chem. Rev.*, 2014, **114**, 11683.

9 D. Aurbach, Z. Lu, A. Schechter, Y. Gofer, H. Gizbar, R. Turgeman, Y. Cohen, M. Moshkovich and E. Levi, *Nature*, 2000, **407**, 724.

10 O. Mizrahi, N. Amir, E. Pollak, O. Chusid, V. Marks, H. Gottlieb, L. Larush, E. Zinigrad and D. Aurbach, *J. Electrochem. Soc.*, 2008, **155**, A103.

11 H. S. Kim, T. S. Arthur, G. D. Allred, J. Zajicek, J. G. Newman, A. E. Rodnyanaky, A. G. Oliver, W. C. Boggess and J. Muldoon, *Nat. Commun.*, 2011, **2**, 1.

12 Y. Liang, R. Feng, S. Yang, H. Ma, J. Liang and J. Chen, *Adv. Mater.*, 2011, **23**, 640.

13 J. Muldoon, C. B. Bucur, A. G. Oliver, T. Sugimoto, M. Matsui, H. S. Kim, G. D. Allred, J. Zajicek and Y. Kotani, *Energy Environ. Sci.*, 2012, **5**, 5941.

14 Y.-S. Guo, F. Zhang, J. Yang, F.-F. Wang, Y. NuLi and S.-I. Hirano, *Energy Environ. Sci.*, 2012, **5**, 9100.

15 F. F. Wang, Y. S. Guo, J. Yang, Y. Nuli and S. Hirano, *Chem. Commun.*, 2012, **48**, 10763.

16 R. Mohtadi, M. Matsui, T. S. Arthur and S.-J. Hwang, *Angew. Chem. Int. Ed.*, 2012, **51**, 9780.

17 J. Muldoon, C. B. Bucur, A. G. Oliver, J. Zajicek, G. D. Allred and W. C. Boggess, *Energy Environ. Sci.*, 2013, **6**, 482.

18 H. D. Yoo, I. Shterenberg, Y. Gofer, G. Gershinsky, N. Pour and D. Aurbach, *Energy Environ. Sci.*, 2013, **6**, 2265.

19 C. J. Barile, R. Spatney, K. R. Zavadil and A. A. Gewirth, *J. Phys. Chem. C*, 2014, **118**, 10694.

20 T. J. Carter, R. Mohtadi, T. S. Arthur, F. Mizuno, R. Zhang, S. Shirai and J. W. Kampf, *Angew. Chem. Int. Ed.*, 2014, **53**, 3173.

21 C. B. Bucur, T. Gregory and J. Muldoon, in *Rechargeable Batteries: Materials, Technologies and New Trends*, Z. Zhang and S. S. Zhang, Editors, Chap. 22, Springer International Publishing, Switzerland, 2015.

22 S.-Y. Ha, Y.-W. Lee, S. W. Woo, B. Koo, J.-S. Kim, J. Cho, K. T. Lee and N.-S. Choi, *ACS Appl. Mater. Interfaces*, 2014, **6**, 4063.

23 D. Aurbach, R. Skaletsky and Y. Gofer, *J. Electrochem. Soc.*, 1991, **138**, 3536.

24 H. J. T. Ellingham, *J. Soc. Chem. Ind.*, 1944, **63**, 125.

25 Z. Rong, R. Malik, P. Canepa, G. S. Gautam, M. Liu, A. Jain, K. Persson and G. Ceder, *Chem. Mater.*, 2015, **27**, 6016.

26 R. D. Shannon, *Acta Cryst.*, 1976, **A32**, 751.

27 D. M. Seo, O. Borodin, S.-D. Han, Q. Ly, P. D. Boyle and W. A. Henderson, *J. Electrochem. Soc.*, 2012, **159**, A553.

28 D. M. Seo, O. Borodin, S.-D. Han, P. D. Boyle and W. A. Henderson, *J. Electrochem. Soc.*, 2012, **159**, A1489.

29 D. M. Seo, O. Borodin, D. Balogh, M. O'Connell, Q. Ly, S.-D. Han, S. Passerini, and W. A. Henderson, *J. Electrochem. Soc.*, 2013, **160**, A1061.

30 S.-D. Han, O. Borodin, J. L. Allen, D. M. Seo, D. W. McOwen, S.-H. Yun and W. A. Henderson, *J. Electrochem. Soc.*, 2013, **160**, A2100.

31 S.-D. Han, O. Borodin, D. M. Seo, Z.-B. Zhou and W. A. Henderson, *J. Electrochem. Soc.*, 2014, **161**, A2042.

32 O. Borodin, S.-D. Han, J. S. Daubert, D. M. Seo, S.-H. Yun and W. A. Henderson, *J. Electrochem. Soc.*, 2015, **162**, A501.

33 N. N. Rajput, X. Qu, N. Sa, A. K. Burrell, K. A. Persson, *J. Am. Chem. Soc.*, 2015, **137**, 3411.

34 C. Xu, H. Du, B. Li, F. Kang and Y. Zeng, *Electrochem. Solid St.*, 2009, **12**, A61.

35 C. Xu, B. Li, H. Du and F. Kang, *Angew. Chem. Int. Ed.*, 2012, **51**, 933.

36 C. Xu, S. W. Chiang, J. Ma and F. Kang, *J. Electrochem. Soc.*, 2013, **160**, A93.

37 J. Lee, J. B. Ju, W. I. Cho, B. W. Cho and S. H. Oh, *Electrochimica Acta*, 2013, **112**, 138.

38 B. Lee, C. S. Yoon, H. R. Lee, K. Y. Chung, B. W. Cho and S. H. Oh, *Scientific Reports*, 2014, **4**, 6066.

39 Z. Jia, B. Wang and Y. Wang, *Mater. Chem. Phys.*, 2015, **149-150**, 601.

40 R. Trcoli and F. L. Mantia, *ChemSusChem*, 2015, **8**, 481.

41 E. Gocke, W. Schramm, P. Dolscheid and R. Schllhorn, *J. Solid State Chem.*, 1987, **70**, 71.

42 N. S. V. Narayanan, B. V. Ashokraj and S. Sampath, *J. Colloid Interface Sci.*, 2010, **342**, 505.

43 T. J. Simons, D. R. MacFarlane, M. Forsyth and P. C. Howlett, *ChemElectroChem*, 2014, **1**, 1688.

44 A. Guerfi, J. Trottier, I. Boyano, I. De Meatza, J. A. Blazquez, S. Brewer, K. S. Ryder, A. Vijh and K. Zaghib, *J. Power Sources*, 2014, **248**, 1099.

45 D. L. Proffit, A. L. Lipson, B. Pan, S.-D. Han, T. T. Fister, Z. Feng, B. J. Ingram, A. K. Burrell and J. T. Vaughey, *MRS Proceedings*, 2015, **1773**, mrss15-2137275.

46 A. L. Lipson, D. L. Proffit, B. Pan, T. T. Fister, C. Liao, A. K. Burrell, J. T. Vaughey and B. J. Ingram, *J Electrochem Soc.*, 2015, **162**, A1574.

47 A. Benmayza, M. Ramanathan, T. S. Arthur, M. Matsui, F. Mizuno, J. Guo, P. Glans and J. Prakash, *J. Phys. Chem. C*, 2013, **117**, 26881.

48 S. Pronk, S. Páll, R. Schulz, P. Larsson, P. Bjelkmar, R. Apostolov, M. R. Shirts, J. C. Smith, P. M. Kasson, D. van der Spoel, B. Hess and E. Lindahl, *Bioinformatics*, 2013, **29**, 845.

49 L. Martínez, R. Andrade, E. G. Birgin and J. M. Martínez, *J. Comput. Chem.*, 2009, **30**, 2157.

50 J. Wang, R. M. Wolf, J. W. Caldwell, P. A. Kollman and D. A. Case, *J. Comput. Chem.*, 2004, **25**, 1157.

51 J. Wang, W. Wang, P. A. Kollman and D. A. Case, *J. Mol. Graphics Modell.*, 2006, **25**, 247.

52 C. I. Bayly, P. Cieplak, W. D. Cornell and P. A. Kollman, *J. Phys. Chem.*, 1993, **97**, 10269.

53 Y. Shao et al., *Mol. Phys.* 2015, **113**, 184.

54 A. I. Krylov and P. M. W. Gill, *Wiley Interdiscip. Rev. Comput. Mol. Sci.*, 2013, **3**, 317.

55 P. J. Stephens, F. J. Devlin, C. F. Chabalowski and M. J. Frisch, *J. Phys. Chem.*, 1994, **98**, 11623.

56 R. Ditchfield, W. J. Hehre and J. A. Pople, *J. Chem. Phys.*, 1971, **54**, 724.

57 J. Tomasi, B. Mennucci and E. Cancès, *J. Mol. Struc. Theochem*, 1999, **464**, 211.

58 X. Qu, A. Jain, N. N. Rajput, L. Cheng, Y. Zhang, S. P. Ong, M. Brafman, E. Maginn, L. A. Curtiss and K. A. Persson, *Comput. Mater. Sci.*, 2015, **103**, 56.

59 S. P. Ong, O. Andreussi, Y. Wu, N. Marzari and G. Ceder, *Chem. Mater.*, 2011, **23**, 2979.

60 J. Qian, W. A. Henderson, W. Xu, P. Bhattacharya, M. Engelhard, O. Borodin and J.-G. Zhang, *Nat. Commun.*, 2015, **6**, 6362.

61 D. Aurbach and Y. Gofer, in *Nonaqueous Electrochemistry*, D. Aurbach, Editor, Chap. 4, Marcel Dekker, Inc., New York, 1999.

62 W. A. Henderson, *J. Phys. Chem. B*, 2006, **110**, 13177.

63 D. R. Lide, Editor-in-Chief, *CRC Handbook of Chemistry and Physics*, 85th Edition, CRC Press LLC, Boca Raton, 2004.

64 C. Wohlfarth, *Landolt-Börnstein IV/25: Viscosity of Pure Organic Liquids and Binary Liquid Mixtures*, M. D. Lechner, Editor, Springer, Berlin, 2009.

65 J. Sullivan, D. Hanson and R. Keller, *J. Electrochem. Soc.*, 1970, **117**, 779.

66 M. S. Ding, *J. Electrochem. Soc.*, 2004, **151**, A40.

Table 1 Electrochemical properties comparison among 16 different non-aqueous Zn electrolytes (for 0.1 M concentration).

		$Zn(TFSI)_2$	$Zn(CF_3SO_3)_2$	$Zn(BF_4)_2$	$Zn(PF_6)_2$
diglyme (G2)	AS[1]	~2.6 V	~2.4 V	n/a	~2.3 V
	CE[2]	n/a	n/a	n/a	100 %
	solubility[3]	lightly cloudy	homogeneous	not soluble	lightly cloudy
	CV[4]	additional redox reactions	additional redox reaction	n/a	additional redox reactions
acetonitrile (AN)	AS[1]	~3.8 V	~3.6 V	~3.8 V	~3.6 V
	CE[2]	99 %	100 %	100 %	n/a
	solubility[3]	lightly cloudy	homogeneous	cloudy	homogeneous
	CV[4]	no additional redox reaction	no additional redox reaction	additional redox reactions	additional redox reactions
propylene carbonate (PC)	AS[1]	~3.4 V	~3.3 V	~3.3 V	~3.3 V
	CE[2]	100 %	100 %	n/a	100 %
	solubility[3]	lightly cloudy	cloudy	cloudy	homogeneous
	CV[4]	additional redox reactions	additional redox reactions	additional redox reactions	additional redox reactions
N,*N*-dimethyl-formamide (DMF)	AS[1]	~2.9 V	~2.8 V	~2.8 V	~2.5 V
	CE[2]	50.8 %	n/a	n/a	100 %
	solubility[3]	lightly cloudy	homogeneous	cloudy	homogeneous
	CV[4]	additional redox reactions	additional redox reactions	additional redox reactions	additional redox reactions

[1]anodic stability.
[2]Coulombic efficiency.
[3]at 25˚C (inhomogenous mixtures with G2, AN, PC and DMF were also stirred/heated on a hot plate up to 80-120˚C considering boiling point of each solvent and decomposition temperature of each salt, but homogeneous solutions could not be created.)
[4]cyclic voltamogram.

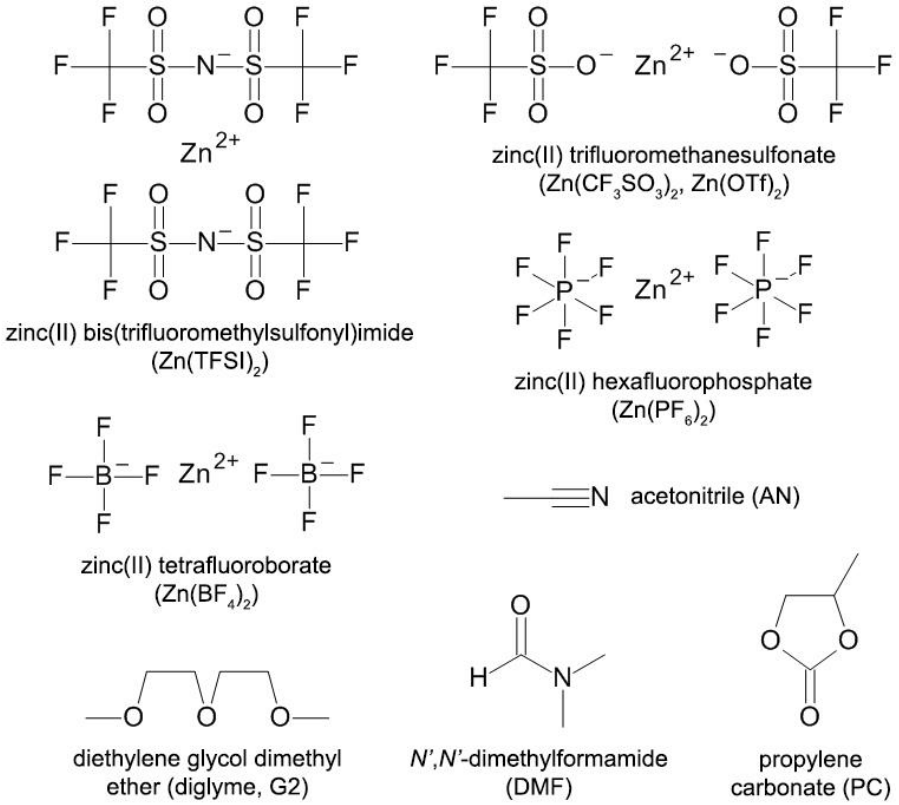

Figure 1. Structures and acronyms of the zinc salts and solvents studied.

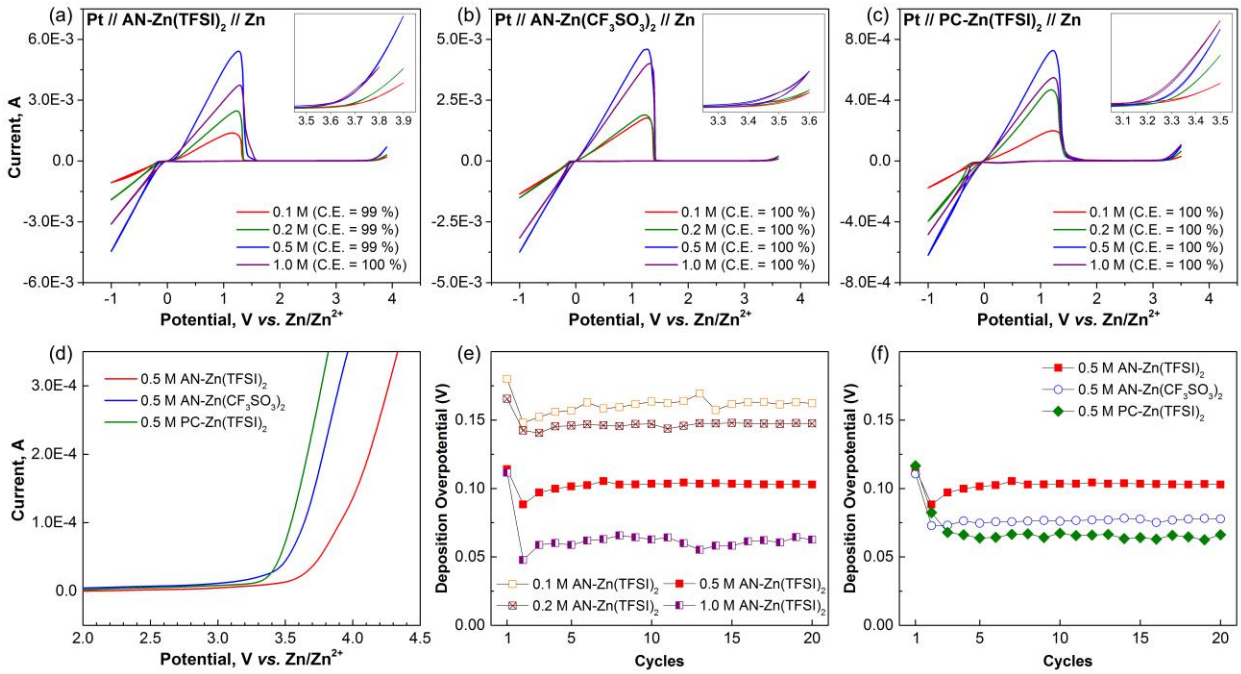

Figure 2. CVs of variable-concentration (a) AN-Zn(TFSI)$_2$, (b) AN-Zn(CF_3SO_3)$_2$ and (c) PC-Zn(TFSI)$_2$ (the scan rate for the CVs was 0.1 V s^{-1}). (d) LSVs of 0.5 M AN-Zn(TFSI)$_2$, AN-Zn(CF_3SO_3)$_2$ and PC-Zn(TFSI)$_2$ electrolytes (the scan rate for the LSVs was 0.025 V s^{-1}). Reversible deposition overpotential of (e) variable-concentration AN-Zn(TFSI)$_2$ and (f) 0.5 M AN-Zn(TFSI)$_2$, AN-Zn(CF_3SO_3)$_2$ and PC-Zn(TFSI)$_2$ electrolytes (the scan rate for the 20 CV cycles was 0.01 V s^{-1}).

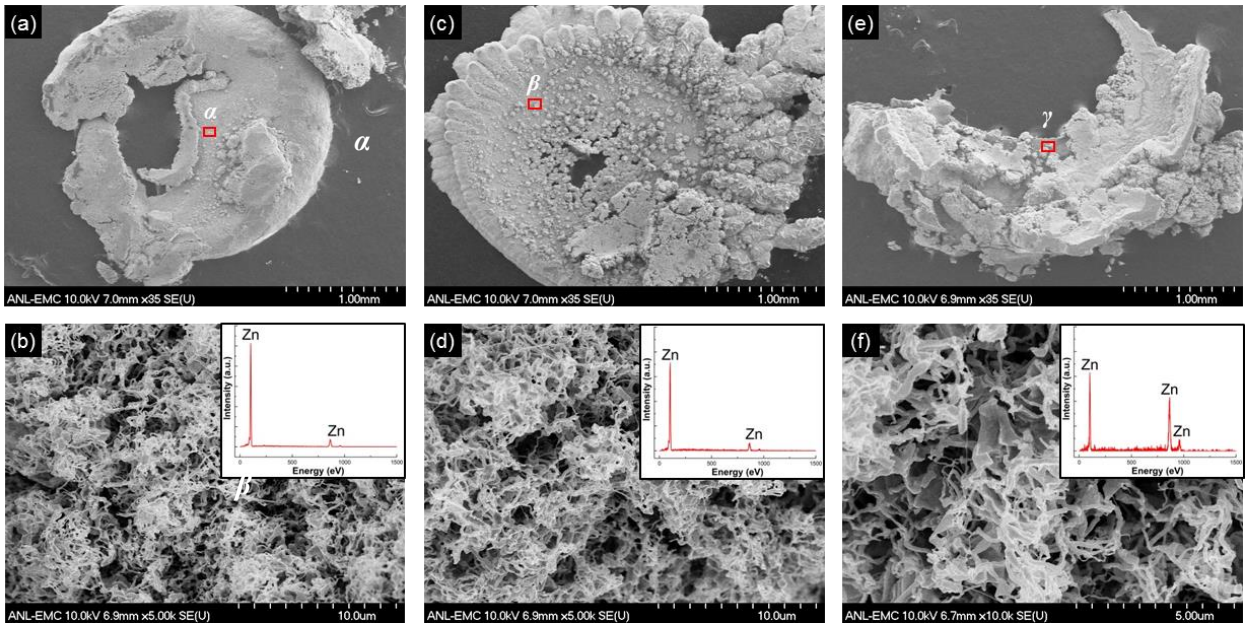

Figure 3. SEM images of (a) Pt electrode after overnight Zn deposition in 0.5 M AN-$Zn(TFSI)_2$ electrolyte, (b) a selected zone α of a, (c) Pt electrode after overnight Zn deposition in 0.5 M AN-$Zn(CF_3SO_3)_2$ electrolyte, (d) a selected zone β of c, (e) Pt electrode after overnight Zn deposition in 0.5 M PC-$Zn(TFSI)_2$ electrolyte and (f) a selected zone γ of e (the insets in Figs 3b, 3d and 3f show the EDS spectrum of Zn deposits).

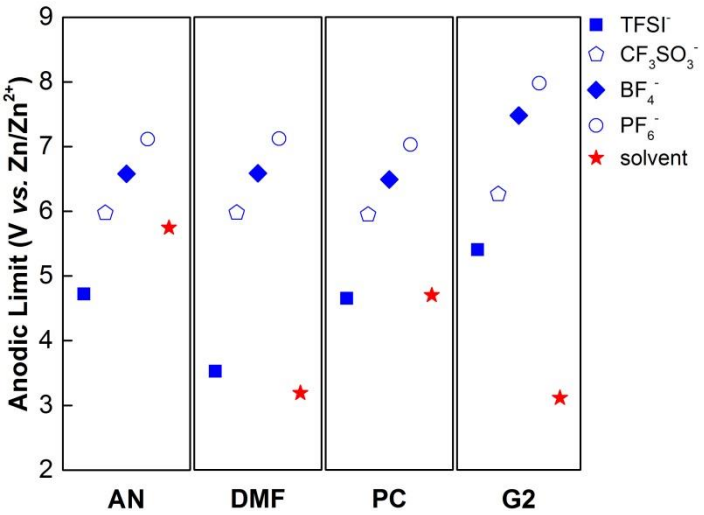

Figure 4. Calculated electrochemical windows (IP) of different salt anions in different solvent dielectric media. All the values are reported *versus* Zn/Zn^{2+}, and the solvent effect is taken into account by the IEF-PCM model. All the anions are listed in the legend and indicated by different symbols.

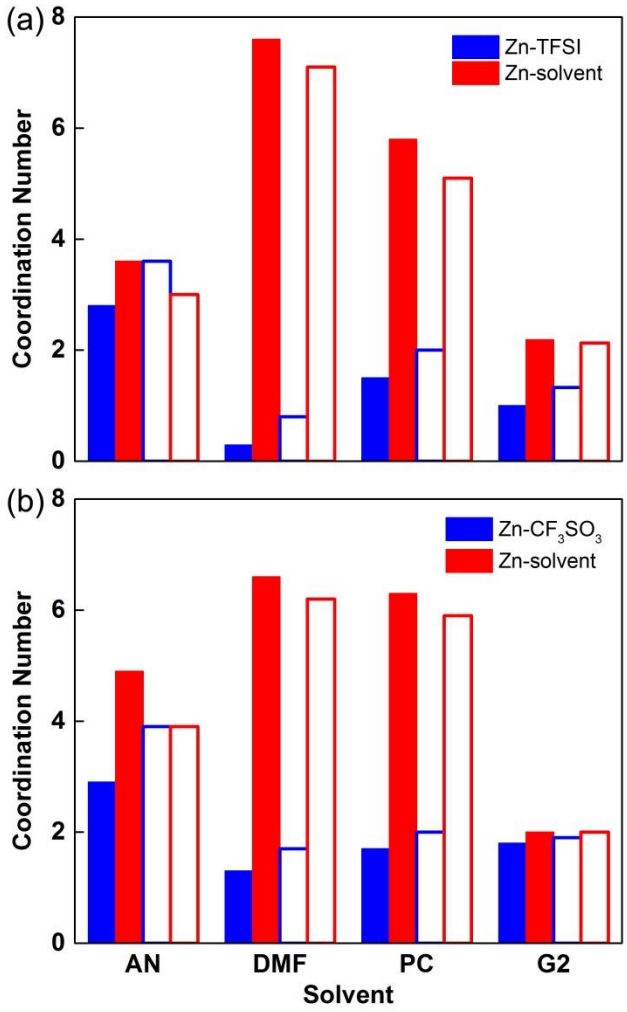

Figure 5. Coordination numbers of Zn-anion and Zn-solvent in the first solvation shell for the (a) $Zn(TFSI)_2$ and (b) $Zn(CF_3SO_3)_2$ electrolytes with four different solvents (0.1 M (filled bars) and 0.5 M (hollow bars) concentrations).

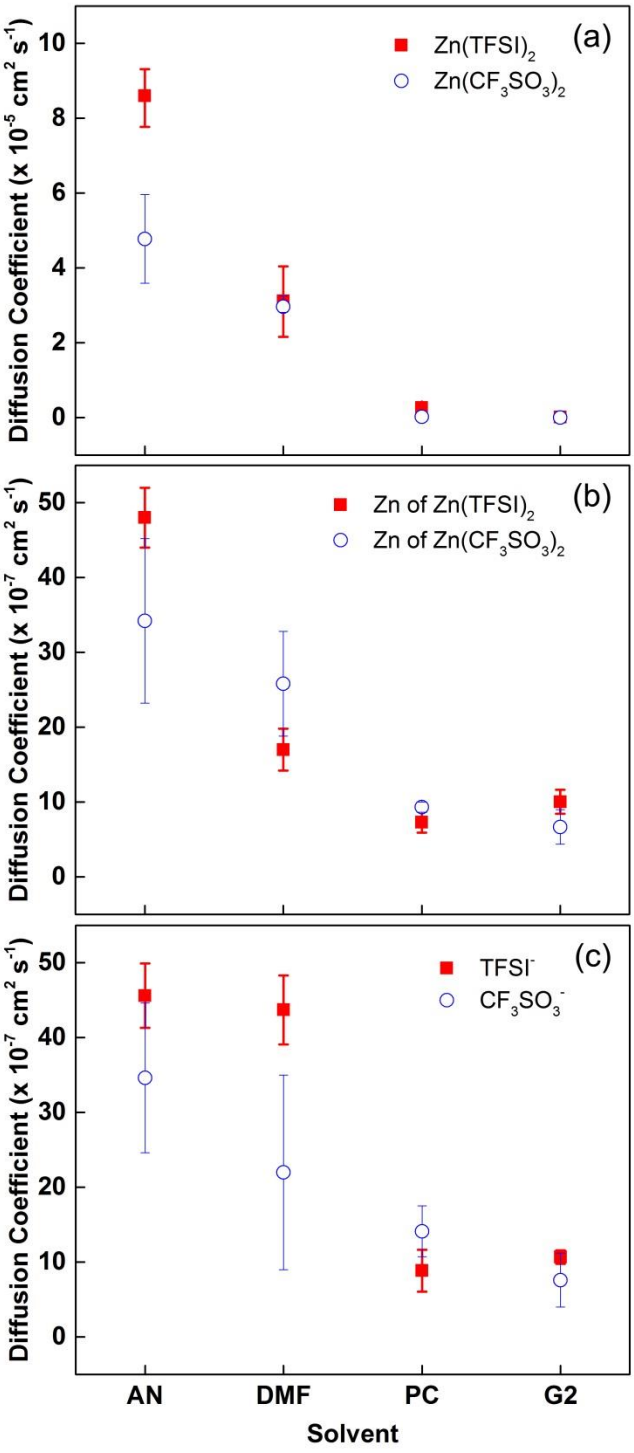

Figure 6. Isothermal diffusion coefficients of (a) $Zn(TFSI)_2$ and $Zn(CF_3SO_3)_2$ (from experimental estimation methods at 25 °C), (b) Zn^{2+} cations and (c) $TFSI^-$ and $CF_3SO_3^-$ anions (from MD simulations at 298 K, error bars were estimated based on the difference of the diffusion coefficients obtained from fits over the two halves of the fit interval) of 0.1 M $Zn(TFSI)_2$ and $Zn(CF_3SO_3)_2$ electrolytes with AN, DMF, PC and G2.

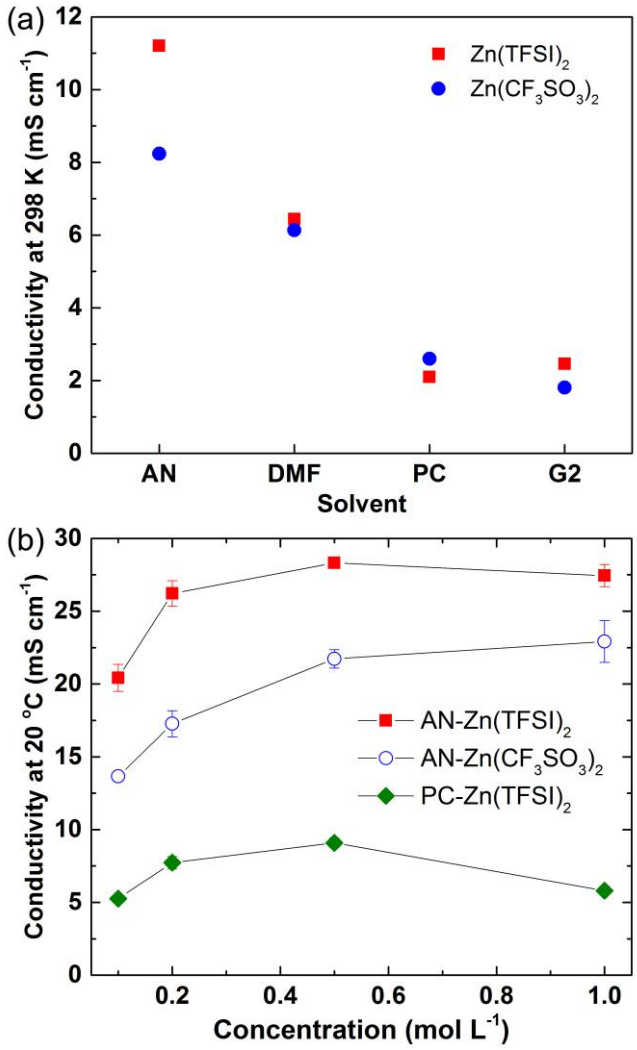

Figure 7. Isothermal ionic conductivities of (a) 0.1 M $Zn(TFSI)_2$ and $Zn(CF_3SO_3)_2$ electrolytes with AN, DMF, PC and G2 (from MD simulations at 298 K) and (b) the AN-$Zn(TFSI)_2$, AN-$Zn(CF_3SO_3)_2$ and PC-$Zn(TFSI)_2$ electrolytes with varying concentration (error bars shown for multiple measurements at 20 °C).